Acoustic attenuation, phase and group velocities in liquid-filled pipes II: Simulation for spallation neutron sources and planetary exploration

Jian Jiang, Kyungmin Baik, and Timothy G. Leighton[a]
Institute of Sound and Vibration Research, University of Southampton, Highfield, Southampton, Hampshire, SO17 1BJ, United Kingdom

This paper uses a Finite Element Method (FEM) to compare predictions of the attenuation and sound speeds of acoustic modes in a fluid-filled pipe with those of the analytical model presented in the first paper in this series. It explains why, when the predictions of the earlier paper were compared with experimental data from a water-filled PMMA pipe, the uncertainties and agreement for attenuation data were worse than those for sound speed data. Having validated the FEM approach in this way, the versatility of FEM is thereafter demonstrated by modeling two practical applications which are beyond the analysis of the earlier paper. These applications model propagation in the mercury-filled steel pipework of the Spallation Neutron Source at the Oak Ridge National Laboratory (Tennessee), and in a long-standing design for acoustic sensors for use on planetary probes. The results show that strong coupling between the fluid and the solid walls means that erroneous interpretations are made of the data if they assume that the sound speed and attenuation in the fluid in the pipe are the same as those that would be measured in an infinite volume of identical fluid, assumptions which are common when such data have previously been interpreted.
© 2011 Acoustical Society of America. [DOI: 10.1121/1.3598463]

I. INTRODUCTION

Acoustic wave propagation in liquid-filled pipes has wide applications in the oil and water industries[1,2] (e.g., for leak detection), and for monitoring product and/or coolant in a range of industries (e.g., in the manufacture of foodstuffs, pharmaceuticals,[3,4] and domestic products such as paints, ceramics, etc.[5,6]). The first stages of this work[7,8] provided an analytical model for predicting both the attenuation and sound speed in a liquid-filled pipe. This was done by extending into the complex domain the pioneering theory of Del Grosso,[9] who gave an exact solution for the axisymmetric modes using elasticity theory. In the low frequency regime for the particular case when the outside of the tube is surrounded by vacuum, Del Grosso's theory was experimentally verified by Lafleur and Shields[10] who measured the phase speeds of the axisymmetric modes inside water-filled PVC and aluminum tubes surrounded by air (quasi-vacuum but regarded as vacuum in the literature) and also presented the analytic solutions at the zero-frequency limit. Del Grosso's theory works well in many applications, but it only considers the real solution for the wave speed, and so cannot take into account attenuation caused by absorption. Later papers described losses in specific scenarios[2,11,12] (thin-walled pipes, low acoustic frequencies) and through a range of mechanisms (radiation into the surrounding medium,[13–15] dissipation through the addition of absorbent liners to the ducts,[16,17] or viscous losses in liquid contained in a lossless pipe wall[18]). However, the key assumptions inherent in these studies do not apply to the mercury-filled steel pipes of the

Spallation Neutron Source (SNS) at the Oak Ridge National Laboratory (ORNL), TN. This is because the sensors operate above the low-frequency limit, mercury has very high thermal conductivity among liquids (very low Prandtl number), and because the pipes cannot be considered thin-walled. Furthermore, the pipes are unlined, and they cannot radiate significantly into the surrounding medium (air). In the consequent absence of losses through liners, radiation or liquid viscosity, the acoustic attenuation is dominated by dissipation through thermal conduction in the liquid and coupling between the viscoelastic liquid and the elastic pipe walls. Such coupling was formulated in the previous paper.[7] It was validated against water-filled pipes, but not the nearly inviscid case of mercury-filled SNS pipes because of safety reasons. The current paper provides this missing validation using a Finite Element Method (FEM), which it then exploits to assess the performance of a proposed planetary acoustic sensor.

Many of the applications listed at the outset of this paper relate to the importance of measuring gas bubbles in pipelines[19,20] or similar cylindrical bodies of liquid,[21,22] and this series of papers aims to produce an acoustic method for doing this. First, however, the acoustic propagation in bubble-free conditions must be characterized to provide a baseline. The first paper[7] in this series showed good agreement between measured and predicted sound speed in the water-filled pipe, but validation of the predicted bubble-free attenuation was less certain because of the uncertainty in measuring the low attenuation seen in bubble-free conditions. This second paper simulates propagation in bubble-free conditions using FEM to provide a comparable exercise for the analytical model of the first paper[7,8] that has less uncertainty than the experimental measurements. Moreover, the FEM is used to generate simulated experimental data in order to test the advantages and

---

[a]Author to whom correspondence should be addressed. Electronic mail: tgl@soton.ac.uk

disadvantages of the candidate methods for processing data. Furthermore, this paper shows how the simulation can be used to test scenarios in ways not previously possible. Two example scenarios are studied. The first scenario is for propagation in the Spallation Neutron Source (SNS) Target Test Facility (TTF) pipework at the Oak Ridge National Laboratory (ORNL), TN. The requirement is to predict the sound speed and attenuation in the ORNL pipework, since the impact of the proton beam on the mercury not only generates neutrons but also produces shock waves which can cause cavitation erosion in the steel. The addition of small helium bubbles to the mercury would attenuate this shock wave,[23,24] and the eventual goal of this project is to be able to predict acoustic propagation in steel pipes of bubbly and bubble-free mercury in order to predict this attenuation, and in order to use acoustic attenuation to monitor the bubble population. The straight-pipe geometry at ORNL is amendable to application of the analytical model of Baik et al.[7,8] to predict the propagation, but the hazardous nature of the environment precludes the acquisition of appropriate experimental data by this team. The efficacy of the FEM in this case is to provide numerical data for this condition when experimental data would be too hazardous to obtain.

The second scenario is for propagation in an acoustical sensor that was proposed for use on Venus and has recently been suggested for use in the atmospheres of gas giants such as Jupiter (in both cases, the dense atmospheres can couple acoustically with the walls of the sensor pipe). In this case the pipe geometry is too complicated to be accessible by the model of Baik et al.,[7,8] and so it is the FEM approach which is used to predict the propagation.

The finite element method is a well-established approach for solving the problem of wave propagation in elastic materials.[25–27] There are two main models that can be used to solve the problem, a time-transient model and an alternative model based in the frequency domain. The time-transient model uses time-marching routines. It solves the equations of dynamic equilibrium and predicts the displacement as a function of time. Since very many temporal iterations are required in this model, the calculation is time expensive. In addition, it does not provide an easy access to input the frequency-dependent attenuation which is key to the scenarios of interest. The alternative approach decomposes the time domain problem into a number of steady state ones in the frequency domain. A time history can be obtained by post-processing the results using an inverse Fourier Transform. Initial studies confirmed the findings of earlier papers[28–30] that the frequency domain model has comparable accuracy, but greatly enhanced speed, compared to the time domain approach. Because of this and the ease with which it accounts for frequency-dependent attenuation, it is the option used here.

In Sec. II the basic equations for dynamic equilibrium in an elastic material are briefly introduced. In Sec. III, the Spallation Neutron Source, which is simplified to a liquid-filled elastic pipe, is investigated. The results are compared to theoretical and experimental studies. In Sec. IV, acoustic wave propagation in a planetary exploration sensor is numerically investigated. Section V provides the conclusions.

II. FORMALISM

The equations of dynamic equilibrium in an elastic material can be expressed as

$$\frac{\partial^2 \vec{S}}{\partial t^2} = (c_c^2 - c_s^2)\nabla(\nabla \cdot \vec{S}) + c_s^2 \nabla^2 \vec{S}, \tag{1}$$

where $\vec{S}$ is displacement, c_c and c_s are the longitudinal velocity and transverse velocity, respectively:

$$c_c = \sqrt{\frac{\lambda + 2\mu}{\rho}}, \quad c_s = \sqrt{\frac{\mu}{\rho}}, \tag{2}$$

where ρ is the density of the medium hosting the waves, and λ and μ are Lame constants.

In the liquid-filled solid-walled pipe, the sound field is assumed to be axisymmetric (while this is a convenient assumption, and in line with the model,[8] note that experimental data[7] in fact suggests the existence of non-axisymmetric modes). In axisymmetric conditions, all derivatives with respect to θ vanish, including the displacement component in the θ direction, the shear strain components $\varepsilon_{r\theta}$ and $\varepsilon_{\theta z}$, and the shear stresses $\sigma_{r\theta}$ and $\sigma_{\theta z}$. Using cylindrical coordinates and assuming that $\vec{S}$ takes the form

$$\vec{S} = \begin{bmatrix} u \\ w \end{bmatrix} = \begin{bmatrix} u_0(r,z)e^{j\omega t} \\ w_0(r,z)e^{j\omega t} \end{bmatrix},$$

(where u and w are radial and axial displacements, respectively, and ω is the angular frequency), Eq. (1) can be decoupled as follows:

$$\begin{cases} -\omega^2 u - c_c^2 \frac{1}{r}\frac{\partial}{\partial r}\left(r\frac{\partial u}{\partial r}\right) - (c_c^2 - c_s^2)\frac{\partial^2 w}{\partial r \partial z} - c_s^2 \frac{\partial^2 u}{\partial z^2} + c_c^2 \frac{u}{r^2} = 0 \\ -\omega^2 w - (c_c^2 - c_s^2)\frac{1}{r}\frac{\partial}{\partial r}\left(r\frac{\partial u}{\partial z}\right) - c_s^2 \frac{1}{r}\frac{\partial}{\partial r}\left(r\frac{\partial w}{\partial r}\right) - c_c^2 \frac{\partial^2 w}{\partial z^2} = 0. \end{cases} \tag{3}$$

Equation (3) states the partial differential equations (PDEs) that are to be considered in the current case of the liquid-filled pipe. In order to define the boundary conditions easily, expressions for the strain tensor E and stress tensor T, in axisymmetric cylindrical coordinates, are also given:

$$E = \begin{bmatrix} \varepsilon_{rr} \\ \varepsilon_{zz} \\ 2\varepsilon_{rz} \\ \varepsilon_{\theta\theta} \end{bmatrix} = \begin{bmatrix} \dfrac{\partial u}{\partial r} \\ \dfrac{\partial w}{\partial z} \\ \dfrac{\partial u}{\partial z} + \dfrac{\partial w}{\partial r} \\ \dfrac{u}{r} \end{bmatrix},$$

$$T = \begin{bmatrix} \sigma_{rr} \\ \sigma_{zz} \\ \sigma_{rz} \\ \sigma_{\theta\theta} \end{bmatrix} = \begin{bmatrix} (\lambda + 2\mu)\dfrac{\partial u}{\partial r} + \lambda\dfrac{\partial w}{\partial z} + \dfrac{\lambda}{r}u \\ \lambda\dfrac{\partial u}{\partial r} + (\lambda + 2\mu)\dfrac{\partial w}{\partial z} + \dfrac{\lambda}{r}u \\ \mu\dfrac{\partial u}{\partial z} + \mu\dfrac{\partial w}{\partial r} \\ \lambda\dfrac{\partial u}{\partial r} + \lambda\dfrac{\partial w}{\partial z} + \dfrac{\lambda + 2\mu}{r}u \end{bmatrix}. \tag{4}$$

Finite element software[31] is used in this study to solve the partial differential equations contained in Eq. (3). None of the models provided with the commercial software (COMSOL) are suitable for the case discussed here. Hence, the original PDE model is used. To use this model, Eq. (3) must be written into a regular form, which is pre-defined in the software, as

$$\nabla \cdot (-C\nabla \vec{S} - \alpha\vec{S} + \gamma) + \beta\nabla\vec{S} + a\vec{S} = f \quad \text{in } \Omega, \tag{5}$$

$$\vec{n} \cdot (C\nabla\vec{S} + \alpha\vec{S} - \gamma) + q\vec{S} = g \quad \text{on } \partial\Omega, \tag{6}$$

$$h\vec{S} = r \quad \text{on } \partial\Omega, \tag{7}$$

where C is the diffusion coefficient, α is the conservative flux convection coefficient, β is the convection coefficient, γ is the conservative flux source term, a is the absorption coefficient, f is the source term, q is the boundary absorption coefficient, g is the boundary source term, and h and r are factors of the Dirichlet boundary condition. The term Ω is the considered domain with boundary $\partial\Omega$, and $\vec{n} = (n_r, n_z)$ is the outward unit vector on $\partial\Omega$. Within COMSOL, all the coefficients and terms in Eqs. (5), (6), and (7) can be functions of spatial coordinates. For a two dimensional case, C is a 4×4 matrix, α and β are 4×2 matrices, γ is a 4×1 matrix, a, h and q are 2×2 matrices, and, f, g and r are 2×1 matrices.

Since the software only supports Cartesian coordinates for this PDE model, the terms introduced by cylindrical coordinates are also put into the parameters. The relevant parameters are expressed as

$$C = \begin{bmatrix} c_c^2 & 0 & 0 & c_c^2 - 2c_s^2 \\ 0 & c_s^2 & c_s^2 & 0 \\ 0 & c_s^2 & c_s^2 & 0 \\ c_c^2 - 2c_s^2 & 0 & 0 & c_c^2 \end{bmatrix}, \quad \beta = \begin{bmatrix} -\dfrac{c_c^2}{r} & 0 \\ 0 & 0 \\ 0 & -\dfrac{c_s^2}{r} \\ -\dfrac{c_c^2 - c_s^2}{r} & 0 \end{bmatrix},$$

$$a = \begin{bmatrix} -\omega^2 + \dfrac{c_c^2}{r^2} & 0 \\ 0 & -\omega^2 \end{bmatrix}, \quad q = \begin{bmatrix} n_r \dfrac{c_s^2}{r} & 0 \\ n_z \dfrac{c_s^2}{r} & 0 \end{bmatrix}. \tag{8}$$

In the case of the planetary exploration sensor, the sound field is considered as a 2D Cartesian space. The relevant equations of dynamic equilibrium can be simplified from (1) as

$$\begin{cases} -\omega^2 u - c_c^2 \dfrac{\partial^2 u}{\partial x^2} - c_s^2 \dfrac{\partial^2 u}{\partial y^2} - c_c^2 \dfrac{\partial^2 v}{\partial y \partial x} + c_s^2 \dfrac{\partial^2 v}{\partial x \partial y} = 0, \\ -\omega^2 v - c_s^2 \dfrac{\partial^2 v}{\partial x^2} - c_c^2 \dfrac{\partial^2 v}{\partial y^2} + c_s^2 \dfrac{\partial^2 u}{\partial y \partial x} - c_c^2 \dfrac{\partial^2 u}{\partial x \partial y} = 0, \end{cases} \tag{9}$$

where u and v are the displacements in the x and y directions, respectively. The relevant parameters in (5) should be

$$C = \begin{bmatrix} c_c^2 & 0 & 0 & c_c^2 \\ 0 & c_s^2 & -c_s^2 & 0 \\ 0 & -c_s^2 & c_s^2 & 0 \\ c_c^2 & 0 & 0 & c_c^2 \end{bmatrix}, \quad a = \begin{bmatrix} -\omega^2 & 0 \\ 0 & -\omega^2 \end{bmatrix}. \tag{10}$$

In both cases, the attenuation is introduced by making c_c and c_s complex-valued, as follows:

$$\tilde{c}_i = \frac{c_i}{1 + j\gamma_i} \quad i = c, s, \tag{11}$$

where γ_c and γ_s are the normalized longitudinal and shear absorption coefficients. Here, the transverse velocity and relevant absorption coefficient, for the liquid and gas investigated in this paper, were considered to be zero, because they are far smaller than the relevant longitudinal values. The complex velocity used here and the complex wave number defined by Baik et al.[7,8] have the relationship $\tilde{k} = \omega/\tilde{c}$, which makes it possible to incorporate into the simulation the parameters used in the analytical model.

III. SPALLATION NEUTRON SOURCE

The pipeline from the SNS TTF is considered to have 12.82 cm internal diameter filled with mercury, and a stainless steel wall of 0.655 cm thickness. However, owing to the safety issues of working with mercury, the early experiments were carried out in a water-filled PMMA pipe. This is because the coupling between the liquid and the walls in a water-filled PMMA pipe is sufficiently similar to that found in the SNS TTF pipelines to show similar modal structures and wavespeeds.[7] (As shown in Table I, the ratio between the compressional wave characteristic acoustic impedances of water and PMMA differs from the equivalent mercury/steel ratio by only about 5%.) Hence, the initial simulation is also conducted for a water-filled PMMA pipe (Fig. 1). In the numerical study, the PMMA pipe dimensions are as in the experiment (1.8 m long, with 4.445 cm inner radius and 0.5 cm wall thickness). A plane source is simulated at the bottom of the water column ($z = 0$), giving a uniform specified displacement across the boundary in order to launch pulses (the $z = 0$ base of the pipe walls is modeled to be fixed with no displacements there). The pulses propagate up the water column, and coupling occurs with the walls. The outer wall of the PMMA pipe (which is surrounded by air in the experiment) is set to be pressure-release in the simulation. The air/water interface at the top of the water column ($z = 1.8$ m) is pressure release, and leads to strong reflections.[7,24] While the simulation can predict these reflections with ease, to produce a simpler picture for the illustrative cases shown here, a highly absorbing boundary (not present in the experiment) is placed at the top of the water column in the simulation to eliminate reflections from there which otherwise would make it more difficult for the reader to identify the modes in Figs. 3, 5, 7, and 11. Other input parameters are shown in Table I.

The modal wavespeeds across a range of frequencies can readily be identified by generating a wideband pulse at the source (Fig. 2). Figure 3 shows a time history map of w,

Water	PMMA	Mercury	Steel[a]
$\gamma_c = 7.8119 \times 10^{-11}$	$\gamma_c = 3.4 \times 10^{-3}$	$\gamma_c = 1.8766 \times 10^{-13}$	$\gamma_c = \gamma_s = 0$
$c_c = 1479$ m/s	$\gamma_s = 5.3 \times 10^{-3}$	$c_c = 1451$ m/s	$c_c = 5675$ m/s
$\rho = 1000$ kg/m^3	$c_c = 2690$ m/s	$\rho = 13500$ kg/m^3	$c_s = 3141$ m/s
$Z_{0c} = 1.48 \times 10^6$ Pa · s/m	$c_s = 1430$ m/s	$Z_{0c} = 1.96 \times 10^7$ Pa · s/m	$\rho = 7900$ kg/m^3
	$\rho = 1190$ kg/m^3		$Z_{0c} = 4.48 \times 10^7$ Pa · s/m
	$Z_{0c} = 3.20 \times 10^6$ Pa · s/m		$Z_{0s} = 2.48 \times 10^7$ Pa · s/m
	$Z_{0s} = 1.70 \times 10^6$ Pa · s/m		

[a]Since the attenuation in steel is very small, it is omitted in our investigation to prevent small differences from zero generating numerical artifacts.

the predicted displacement in the axial (z) direction, at center positions of the pipe along the z axis. At least two propagation modes (marked as "a" and "b") can be recognized from Fig. 3. They each represent the lower boundary of their respective wave patterns, and do not pass through the origin because the excitation signal occurs at 0.1 ms [see Fig. 2(a)]. The pattern in each mode shows that the signal is dispersive (the phase velocity depends on frequency, and the pulse duration increases during propagation, e.g., from ~0.1 ms at $z = 0$ to 0.3 ms at $z = 1.8$ m).

The time histories at four example positions, $z = 0$, 0.5, 1, and 1.5 m, are shown in Fig. 4. At the $z = 0$ m position, there is only one major pulse signal showing at around 0.1 ms. When this signal propagates to $z = 0.5$ m, via different modes, it shows two major pulses (the first, labeled "a," arrives at ~0.5 ms, and the second, labeled "b," arriving ~0.3 ms later, the labels indicating correspondence with the modes labeled in Fig. 3). When the signal propagates to $z = 1$ m, the signal corresponding to mode b is about 0.8 ms delayed from that of mode a. The signals in Figs. 3 and 4 illustrate the characteristics of wave propagation inside the water-filled PMMA tube, but they are not appropriate for estimating the phase velocity or the attenuation, because

these signals have a wide frequency band and they are dispersive. To highlight the propagation mode, a 2D Fourier Transform is applied to the data of Fig. 3. It changes the $z - t$ (displacement against time) domain signal to one in the $k - \omega$ (wave number against angular frequency) domain. Since phase velocity is given by $c = \omega/k$, this result can be easily transferred to a domain of phase velocity against wave number (the group velocity can then be obtained by Eq. (3.3) of Baik et al.[8]). A normalized result is shown in Fig. 5. The x axis represents the product of the real part of the wave number in the liquid (k_1) and the inner radius of the pipe (b). The y axis represents the ratio of the phase velocity (C_{0m}) to the speed of sound in the water (C_W). The experimental data from Baik et al.[7] are also plotted on the figure (using the mode labeling convention ET1, ET2, etc., described in the earlier paper), and the agreement between these and the simulation validates the latter. This is particularly so as it implies agreement of the simulation with both analytical model and experiment, since these last two were shown to agree in the earlier paper.[7]

However, the comparison between the analytical model and experiment for attenuation did not show such precise agreement in the earlier paper[7] because of the large error bars in the experimental data (Fig. 10 of Baik et al.[7]), such that any comparison of the analytical model with the
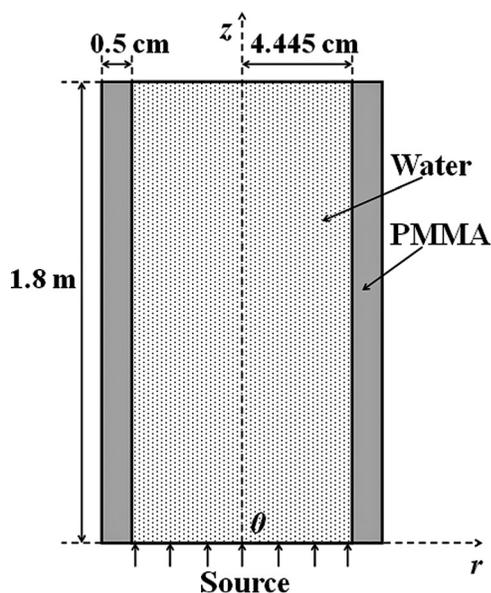

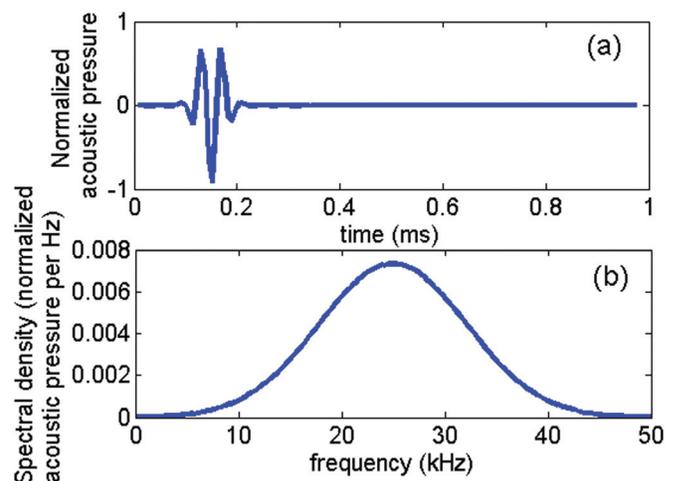FIG. 1. Geometrical dimensions of the water-filled PMMA pipe (not drawn in scale).

FIG. 2. (Color online) Waveform and spectrum of a typical impulse signal. Throughout this whole paper the constant for normalization relating to the "normalized acoustic pressure" is unchanged.
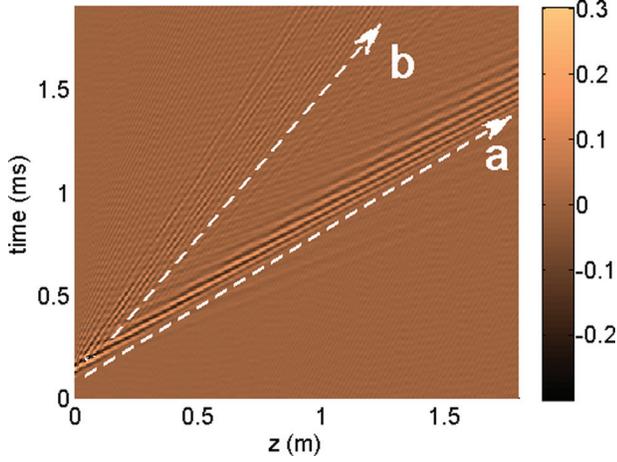
FIG. 3. (Color online) Time history map of w for the signal of Fig. 2 (the study was carried out in a water-filled PMMA pipe whose geometrical dimensions are shown in Fig. 1). Color scale shows the normalized acoustic pressure [as in Fig. 2 (a)] in linear representation. Signals are calculated for the center of the pipe cross section, using the frequency domain method. See supplementary material in Ref. 55 for a movie of a pulse signal propagating though water filled PMMA pipe, calculated using the alterative time-transient method. It can also be found at the web page http://www.isvr.soton.a-c.uk/fdag/PIPE_DEMO/index.htm (last viewed 23 March 2011).

simulations of this paper is particularly important. To make this comparison, the phase spectrum (PS) method (described by Baik *et al.*[7]) is used to extract from the numerical data the attenuation coefficient (which is the imaginary part of the complex wave number). The PS method compares signals collected from two positions along the pipe in the frequency domain. The speed of sound is then given by considering the phase difference between these two signals and the attenuation is given by considering the change of amplitude. However, one drawback of the PS method is that it adds the attenuation from all the modes at a particular frequency together. Therefore the result is actually a sum of the attenuation from all the modes, and the attenuation of each individual mode cannot be inferred unless the signals from the modes are themselves first separated.[7] To overcome this problem, a narrowband signal (quality factor, $Q = f_0/\Delta f$,
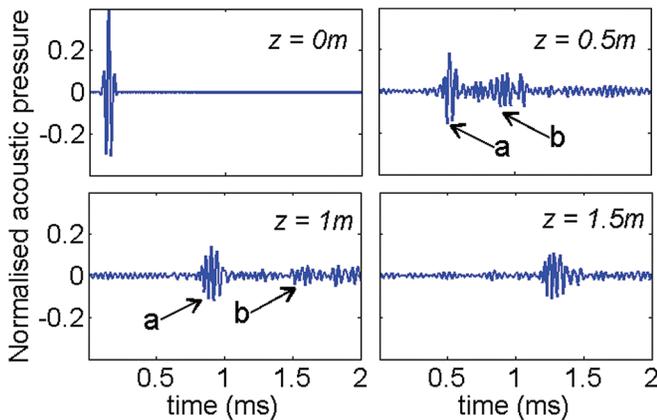

FIG. 4. (Color online) The time domain waveform at different positions for the input shown in Fig. 2(a) (the study was carried out in a water-filled PMMA pipe whose geometrical dimensions are shown in Fig. 1).
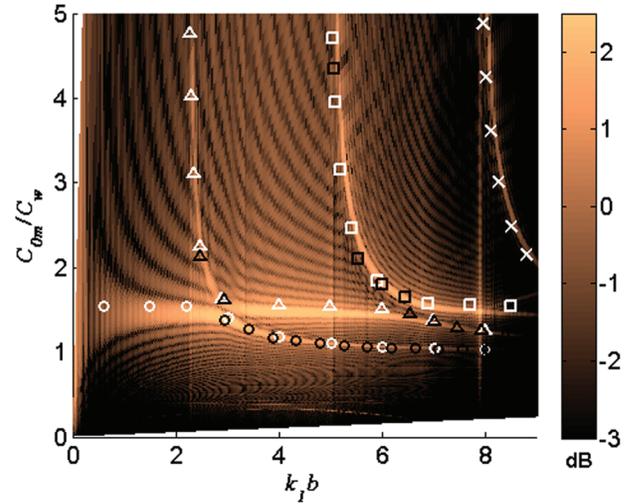

FIG. 5. (Color online) 2D spectrum with axis of normalized phase velocity against normalized wave number (the study was carried out in a water-filled PMMA pipe whose geometrical dimensions are shown in Fig. 1). Since the color scale value is the output of a 2D FFT of data such as that found in Fig. 2, it shows (in dB) the "normalized acoustic pressure per Hz per meter," where 0 dB corresponds to the situation where the original output of 2D FFT equals 1 Hz^{-1} m^{-1}. Circles, triangles, squares, and crosses represent ET1, ET2, ET3, and ET4 modes, respectively. White symbols correspond to theoretical results and black symbols correspond to experimental results.

where f_0 is the center frequency and Δf is the band width which equals 2 kHz here) is used as the pulse signal, and the length of pipe is extended to 10 m, which is long enough to separate the modes (with different propagation speeds) in time domain. The results are shown in Fig. 6.

Figure 6 shows the normalized attenuation for the ET1 and ET2 modes. Variables k_1 and Im$[q_{0m}]$ in the figure were introduced by Baik *et al.*[7] and retained here to ensure consistency across the papers in this series. The parameter k_1 is the real part of the wave number in the liquid, and Im$[q_{0m}]$ is the
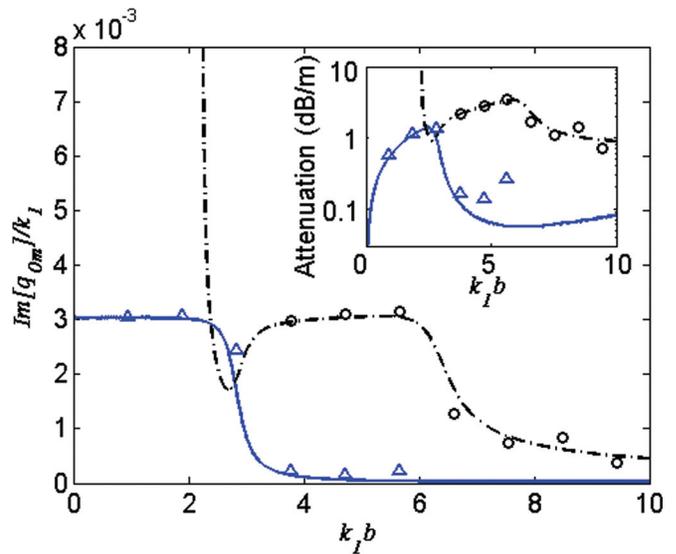

FIG. 6. (Color online) Normalized attenuation plotted against k_1b (the study was carried out in a water-filled PMMA pipe whose geometrical dimensions are shown in Fig. 1). Here Im$[q_{0m}]$ is the imaginary part of wave number which is used in Ref. 7. The solid and dashed lines represent ET1 and ET2 modes, respectively, from the analytical model. The triangles and circles represent ET1 and ET2 modes from the simulation.
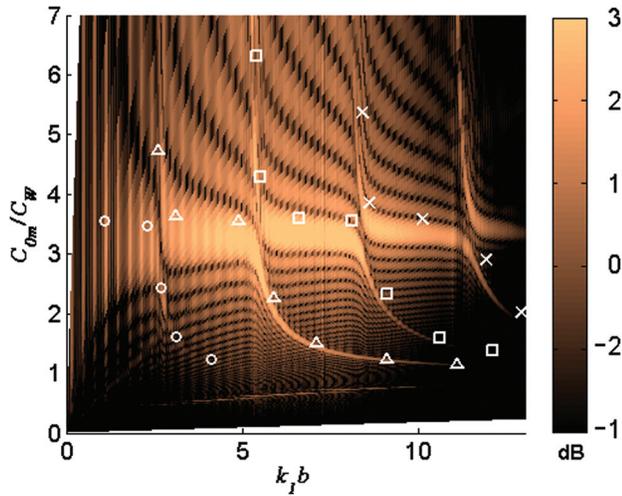
FIG. 7. (Color online) A 2D spectrum with axis of normalized phase velocity against normalized wave number for the steel pipe (wall thickness 0.655 cm) containing mercury to an inner diameter of 12.82 cm. The color scale value (see Fig. 5) is the output of a 2D FFT and shows (in dB) the "normalized acoustic pressure per Hz per meter," where 0 dB corresponds to the situation where the original output of 2D FFT equals 1 Hz^{-1} m^{-1}. Circles, triangles, squares, and crosses represent ET1, ET2, ET3, and ET4 modes, respectively.

imaginary part of the axial wave number, q_{0m}, where "0" refers to axisymmetric mode and "m" refers to the mode index. The ratio between Im[q_{0m}] and k_1 is used here to quantify the attenuation of different modes (shown in the inset to Fig. 6). Small differences are caused by the limited accuracy in distinguishing modes in the time domain. Although the method works well for the simulated 10 m pipe, the 1.8 m pipe used in the experiments is insufficiently long to separate out the modes in the time domain. Baik *et al.*[7] used Prony's method to eliminate the overlap between modes, but the technique resulted in large error bars. This may not be such a problem in the eventual application of using the formulation of Baik *et al.*[7] and the FEM of this paper to model bubble-induced attenuation, since the values of the latter are so much higher than the values for the bubble-free case seen here, so that the proportional effects of uncertainties are decreased. If it does remain a problem, then the attenuation parameters will have to be extracted out from the k-ω map by solving a nonlinear equation set using complex regularization.

From Fig. 3 to Fig. 6, the simulation results have shown that the model developed by Baik *et al.*[7] can be used to predict the propagation modes and attenuation. The simulation will now be used to predict the wave propagation in a mercury-filled steel pipe where the experiment is very difficult to carry out. The 2D spectrum of Fig. 7 plots the normalized phase velocity against the normalized wave number for the steel pipe (wall thickness 0.655 cm) containing bubble-free mercury to an inner diameter of 12.82 cm. The spectrum highlights the propagation modes and shows agreement between the FEM and the model of Baik *et al.*[7] However, while the analytical model could be used to predict attenuation in bubble-free mercury-filled pipelines,[7] one limitation of the simulation is that it cannot do this, because the attenuation in bubble-free mercury-filled steel pipes is such that

(Im[q_{0m}]/k_1) is of the order 10^{-8} (according to Fig. 12 in Ref. 7), which is much smaller than the 10^{-5} accuracy that the current simulation can give. When the attenuation of mercury in pipelines is increased by the addition of bubbles, this problem should be less, and future papers will examine this scenario. While the FEM approach therefore has limitations in some respects compared to the analytical model, it nevertheless offers advantages, such as the fact that it can readily be adapted to predict propagation in the specific geometry of the SNS TTF pipeline (Fig. 8).

IV. ACOUSTIC PLANETARY EXPLORATION SENSOR

Despite the complementary and sometimes unique capabilities which acoustics affords for exploration on alien planets (Mars,[32,33] Titan,[34–37] Europa,[38,39] etc.), acoustical sensors have been far less supported than imaging systems for planetary probes, and have never succeeded in recording the soundscape of an alien atmosphere.[40–42] The *Cassini-Huygens* mission was however extremely successful in measuring the sound speed and attenuation in Titan's atmosphere,[43] and indeed the first sensors for planetary probes were designed to measure similar properties. However, the historically low success rate of acoustical sensors raises the question of optimizing the design of sensors for alien worlds. Such design is a challenging task (including constraints in size, weight, power consumption, data transmission, and the requirement to survive transportation, radiation, etc.) even before acoustical considerations are raised. However, one problem with acoustical design is that the familiarity of using acoustical sources and sensors in Earth's atmosphere may cause subtle yet potent acoustical features to be overlooked when transposing systems that were designed, tested, and calibrated on Earth to other worlds. One example arises through atmospheric fluid loading,[44] which would increase the resonance frequency of a vibrator on Mars compared to an Earth-based calibration, but decrease it on Venus, differences which are important if, say, reductions in that frequency are interpreted as being caused by the minute accumulation of matter on a vibrating plate.[44,45]

The coupling issue discussed so far in this paper is usually small for gas-filled vessels on Earth, but in the dense atmosphere of other worlds, coupling may occur.[40,44] The characteristic acoustic impedance of gas on Venus is about 60 times larger than air on Earth (Table II). One of the earliest designs for an acoustic planetary exploration sensor is a device intended to investigate an alien atmosphere by measuring its speed of sound and acoustic impedance. Hanel and Strange[46,47] proposed applying the well-developed Earth-based technique of measuring the speed of sound by comparing acoustic phase at two different positions along a pipe (which is principally the same as the phase spectrum method mentioned in Sec. III). To save space on a planetary probe, it was designed to be a spiral pipe.[46,47] However, Leighton[44] recently demonstrated how application of familiar Earth-based acoustical techniques to dense extraterrestrial atmospheres, particularly when the transducers are placed within pipes, could generate significant fluid loading. This would affect, for example, the calibration of sensors and sources
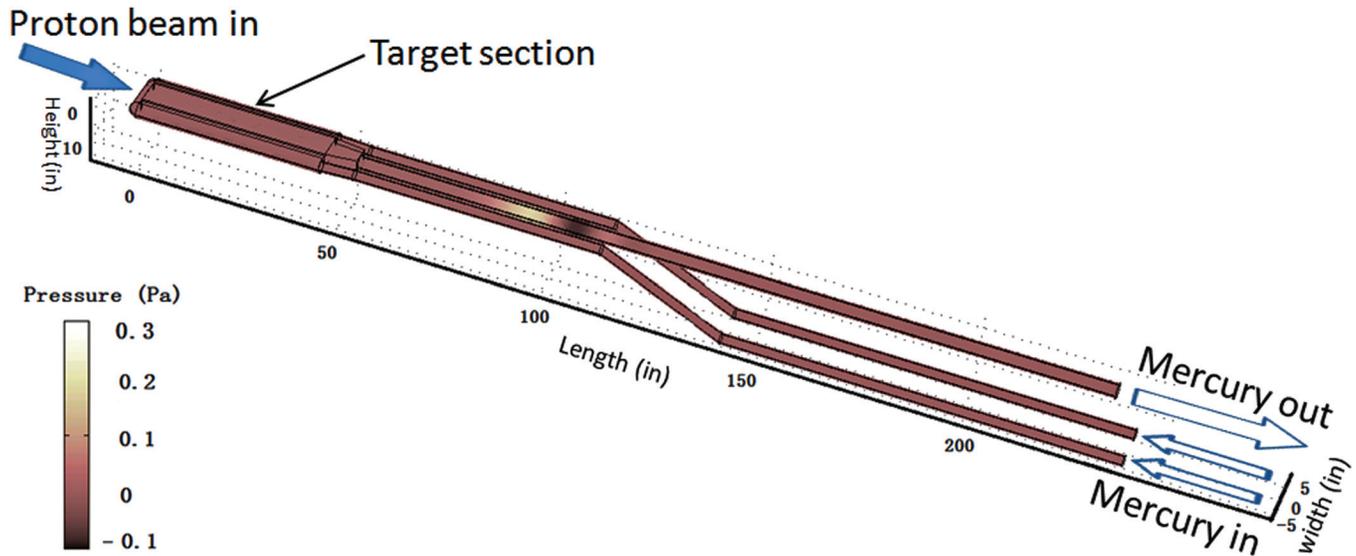
FIG. 8. (Color online) Still (at $t = 2.5$ ms) taken from a movie simulating the propagation of an acoustic pulse in ORNL's SNS Target Test Facility (TTF). As in the simulation, the SNS TTF pipeline consists of a target section (the chamber at the left of the simulation, where the proton beam impacts the mercury). Mercury is pumped into the target section through the two outer pipelines (each of which contains an offset bend to raise the level of the mercury by 23 inches to the height of the target section). The return flow is via the central pipeline. In the existing test loop, the return pipe also contains an offset bend matching those on the inflow pipes. This particular simulation was undertaken to test the possibility of keeping the return flow at the height of the target section in order to facilitate propagation of acoustic pulses along the return pipe toward the target section, in order to measure the bubble population there (the topic of a future paper). See supplementary material in Ref. 55 for a movie of this simulation. It can also be found at the web page http://www.isvr.soton.ac.uk/fdag/PIPE_-DEMO/index.htm (last viewed 23 March 2011).

placed in those pipes. Questions were also raised regarding the effect of coupling on such devices.[40,44] The current paper will show that the spiral pipe geometry is indeed prone to complications caused by coupling.

Since weight, space, ruggedness, and power consumption are key drivers in the design of planetary explorers, the use of strong light materials (which need to be physically and chemically robust for environments such as Venus) is paramount. The initial design[46,47] for the spiral sensor proposed using aluminum for the walls, although today carbon fiber might be seen as a better choice for many environments. The sensor was initially proposed for Venus and its popularity remains current, with proposals to deploy it in future missions to the Jovian planets (Jupiter, Saturn, Uranus, and Neptune).[48] When such techniques have been applied on Earth, the severe impedance mismatch between the construction material and the atmosphere have been assumed to prevent significant coupling, in which case the sound speed and attenuation measured in the pipe should be

very similar to those of the bulk atmosphere. In the dense atmospheres of Venus or a gas giant, coupling will occur, and if the measurements are inverted using the propagation equations and physics/chemistry relationships developed for use in an infinite homogeneous body of gas, then the inferred values will be incorrect. In proposing the use of the spiral pipe for Venus, Hanel[47] writes: "The velocity of sound in a gas c is a function of T [temperature], M [molecular weight], and γ [specific heat ratio], and is given by $c^2 = \gamma R T / M$, where R is the gas constant. This well-known relation has been used in the past in various techniques to measure the temperature $[(T)]$ of Earth's atmosphere, where M and γ were accurately known. It is proposed to reverse this method and bring a volume of the atmosphere of Venus into a thermostatically controlled tube where the temperature is known accurately and to determine M/γ by measuring the velocity of sound through the medium in the tube." It should be noted that such ideal gas treatments would need to be corrected by use of a non-ideal Equation of State if the technique were to

TABLE II. The densities and wave speeds that are used as input parameters for the simulations of an acoustic planet sensor (specific acoustic impedances for compressional waves (and, for solids, the equivalent for shear waves) are also shown for the isotropic materials, though these are not input parameters).

Air on the Earth	Gas on Venus	Steel	Aluminum	Carbon fiber[54]
$c_c = 340$ m/s	$c_c = 410$ m/s	$c_c = 5675$ m/s	$c_c = 6402$ m/s	$c_{11} = 60 + 1.8j$ GPa
$\rho = 1.29$ kg/m³	$\rho = 65$ kg/m³	$c_s = 3141$ m/s	$c_s = 3103$ m/s	$c_{22} = 12 + 0.4j$ GPa
$Z_{0c} = 438.6$ Pa·s/m	$Z_{0c} = 2.67 \times 10^4$ Pa·s/m	$\rho = 7900$ kg/m³	$\rho = 2700$ kg/m³	$c_{12} = 9 + 0.3j$ GPa
	γ_c[a]	$Z_{0c} = 4.48 \times 10^7$ Pa·s/m	$Z_{0c} = 1.73 \times 10^7$ Pa·s/m	$c_{66} = 5 + 0.1j$ GPa
		$Z_{0s} = 2.48 \times 10^7$ Pa·s/m	$Z_{0s} = 8.38 \times 10^6$ Pa·s/m	$\rho = 1500$ kg/m³
			$\gamma_c = 8.50 \times 10^{-5}$	
			$\gamma_s = 2.57 \times 10^{-5}$	

[a] $\gamma_c = \frac{c_c}{\omega} [5.4661 \times 10^{-11} \times (\frac{\omega}{2\pi})^2 + 1.2087 \times 10^{-5} (\frac{\omega}{2\pi}) + 0.0188]$, where ω is angular frequency in radians per second.

be applied to high pressure atmospheres found at ground level on Venus and Titan, and those which a probe might encounter in exploration of the gas giants.[49,50] Departures from a continuum model should be considered if the Knudsen number is high.[51]

Compared to the ground-level atmosphere on Earth, that of Venus (96% CO_2, 3.5% N_2 and 150 ppm SO_2)[52,53] is about 50 times more dense ($\sim$65 kg/m^3 compared to Earth's $\sim$1.29 kg/m^3) and its speed of sound is greater ($\sim$410 m/s on Venus and $\sim$340 m/s on the Earth). The increased density and sound speed of the ground-level atmosphere of Venus give it a specific acoustic impedance (2.67×10^4 Pa$\cdot$s/m) that is a 60 times larger than that found on Earth (438.6 Pa$\cdot$s/m), and hence there is greater potential for coupling to the materials from which the probe is constructed. Here, a simulation is carried out to show that a sensor calibrated on the Earth may not work appropriately on Venus unless such coupling is accounted for, i.e., if the propagation measurements are interpreted as being characteristic of the bulk atmosphere outside of the probe sensor.

Two sensor shapes are investigated in the simulation. One is a straight pipe which is similar as the one shown in Fig. 1 but of different size (2 m long, with 1 cm inner diameter and 1 cm wall thickness) and material (steel, aluminum, and carbon fiber). While this is a less convenient shape for a planetary probe than is the spiral (the second geometry used, with a gas channel 2 m in length; Fig. 9), the straight pipe does provide a useful comparison.

Three different kinds of material are considered for the construction of the straight pipe, including steel, aluminum and carbon fiber. The parameters for steel and aluminum in a 2D Cartesian space have been given in Eq. (10). However, they are more complicated for carbon fiber which is an anisotropic viscoelastic material.[54] To simplify the parameters used for the carbon fiber simulations, the propagation of the acoustic wave is assumed to be within a plate where the plane of propagation is symmetric, with the x direction perpendicular to the plate and the y direction parallel to the direction of fibers. Since only two dimensions are considered, the component on the relevant z direction is 0. The strain tensor E and the stress tensor T can then be simplified as

$$E = \begin{bmatrix} \varepsilon_x \\ \varepsilon_y \\ 2\varepsilon_{xy} \end{bmatrix} = \begin{bmatrix} \dfrac{\partial u}{\partial x} \\ \dfrac{\partial v}{\partial y} \\ \dfrac{\partial u}{\partial y} + \dfrac{\partial v}{\partial x} \end{bmatrix},$$

$$T = \begin{bmatrix} \sigma_x \\ \sigma_y \\ \sigma_{xy} \end{bmatrix} = \begin{bmatrix} c_{11} & c_{12} & 0 \\ c_{12} & c_{22} & 0 \\ 0 & 0 & c_{66} \end{bmatrix} \begin{bmatrix} \dfrac{\partial u}{\partial x} \\ \dfrac{\partial v}{\partial y} \\ \dfrac{\partial u}{\partial y} + \dfrac{\partial v}{\partial x} \end{bmatrix}, \quad (12)$$

where c_{11}, c_{12}, c_{22}, c_{66} are complex viscoelaticity moduli introduced by Hosten et al.[28–30] The parameter C defined in (5) should in such cases be changed to

$$C = \begin{bmatrix} c_{11} & 0 & 0 & c_{12} \\ 0 & c_{66} & c_{66} & 0 \\ 0 & c_{66} & c_{66} & 0 \\ c_{12} & 0 & 0 & c_{22} \end{bmatrix} * \rho^{-1}. \quad (13)$$

The input parameters are shown in Table II.

Figure 10 shows the simulation results of phase velocity in a straight pipe. Here the frequency band is from 2 kHz to 14 kHz, which ensures that (1) the length of the sensor is larger than at least eight wavelengths of the signal, and (2) the frequency is less than the theoretical cut-off frequency that the first higher-order mode would have in an idealized rigid-walled pipe of the same dimensions for the ground-level atmospheres of Earth (17 kHz) and Venus (20 kHz) (this ensures that the received data are not complicated by
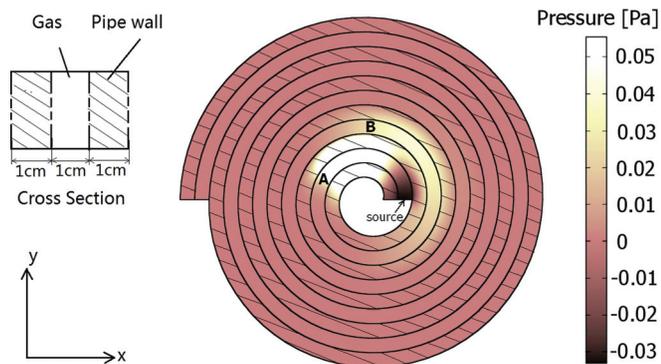

FIG. 9. (Color online) A frame (at t = 0.2 ms after the emission of the pulse by the source) taken from a movie showing an impulse signal generated at the source end of the spiral shape planet exploration sensor and propagating along it. The hatched arm of the spiral is solid, the unhatched arm is gaseous. The inset shows the geometrical dimensions of the channel as relate to this 2D simulation (such that the height of the channel, shown as a dashed line) is not included in the simulation. See supplementary material in Ref. 55 for a movie of this simulation. It can also be found at the web page http://www.isvr.soton.ac.uk/fdag/PIPE_DEMO/index.htm (last viewed 23 March 2011).
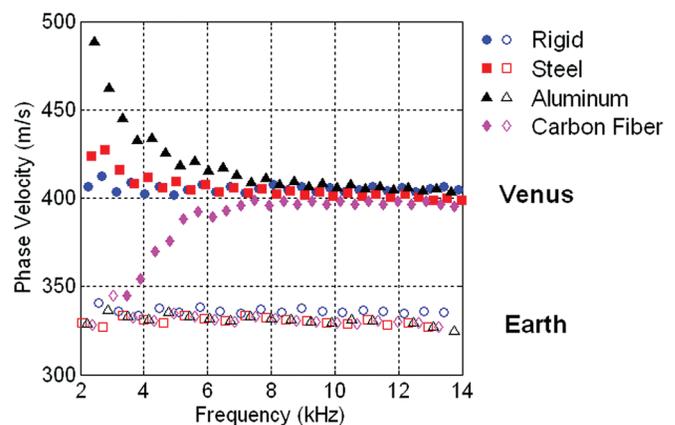

FIG. 10. (Color online) Phase velocity measured by planet sensor (straight pipe). Circles, squares, triangles, and diamonds represent idealized rigid boundary, steel, aluminum, and carbon fiber, respectively. The open symbols correspond to air on the Earth and filled symbols correspond to gas on Venus.

modes other than the lowest one modeled, which would be a sensible precaution in an experimental probe). On the Earth, the coupling between air and the sensor walls is very weak, and so the measurement from Fig. 10 would give a result of around 340 m/s for the straight pipe, in agreement with the value for the bulk atmosphere on Earth which was input into the simulation. However, when the sensor is used on Venus, only the steel pipe gives results resembling those from an idealized rigid boundary: it measures a sound speed for the gas in the pipe which differs from that of the bulk atmosphere by less than 2.5%. Such a percentage change might be considered small in some circumstances, although this degree of coupling to a steel pipe would cause tuning problems if this straight pipe were part of a tuned system (such as a mass sensor[45] or sound source/receiver[40–44]). The coupling problems are much greater if, instead of steel, carbon fiber or aluminum were used. Both aluminum and carbon fiber pipes show dispersion in the straight pipe, because the coupling between sensor wall and gas inside changes the propagation mode of the acoustic wave. The corresponding 2D spectra are shown in Fig. 11 to highlight the propagation mode in [Fig. 11(a)] aluminum and [Fig. 11(b)] carbon fiber straight pipes, respectively.

Figure 12(a) shows the results for a spiral pipe having the dimensions shown in Fig. 9. Two kinds of material, steel and aluminum, are investigated (the anisotropy of carbon fiber precludes its inclusion in this geometry with current computational facilities, although extrapolation from the straight pipe example suggests significant effects from coupling). Since the wall of the spiral pipe is influenced by the gas on both sides (it is similar to a multi-layer sandwich structure excited by signals with different phases) their coupling is very complicated. A snapshot of the sound field at 0.2 ms after a pulse signal was generated at the source end of the gas column is also shown in Fig. 9. At this time, the original wave front that traveled through the gas column has just reached position "A." However, some energy has propagated though the solid walls of the spiral (the hatched areas) to "B." The coupling between gas and solid has allowed energy to bypass the through-gas propagation path between A and B (which is as yet unperturbed). In this way, acoustic energy has traveled through the wall to couple the two gas layers which "sandwich" that portion of wall. Despite the complexity of the sound field inside, Fig. 12(a) shows that
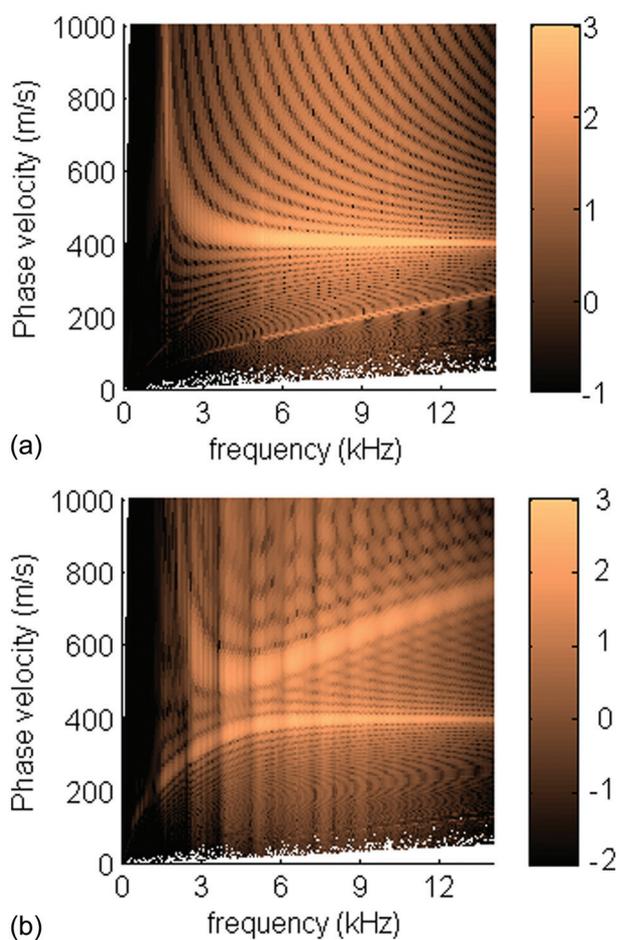

FIG. 11. (Color online) Plots of the 2D spectrum with axis of phase velocity against frequency for straight pipes with 1 cm thick walls of (a) aluminum and (b) carbon fiber containing gas on Venus to an inner diameter of 1 cm. The color scale value which is the output of a 2D FFT shows (in dB) the "normalized acoustic pressure per Hz per meter," where 0 dB corresponds to the situation where the original output of 2D FFT equals 1 Hz^{-1} m^{-1}.
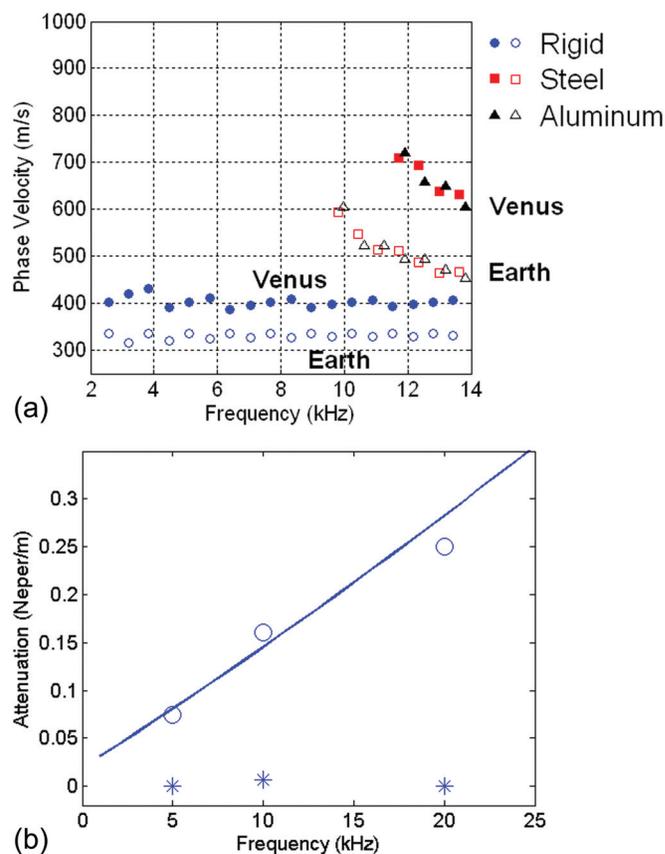

FIG. 12. (Color online) Simulated resulted for measurements of ground-level atmospheres by straight and spiral pipe sensors where the solid walls are made of aluminum. (a) Phase velocity as a function of frequency, as measured by a spiral sensor having the dimensions of Fig. 9. Circles, squares, and triangles represent idealized rigid boundary, steel and aluminum, respectively. The open symbols correspond to the ground-level atmosphere on Earth and filled symbols correspond to that on Venus. (b) The attenuation per unit length, plotted against frequency, as if measured and averaged from 500 microphones placed equidistantly along the axis of the gas column. The solid line shows the input attenuation coefficient of gas on Venus. Circles and stars represent the results measured by using straight and spiral shape sensors, respectively.

use of the phase spectrum method[7] (Sec. III) to obtain the phase velocity indicates that the spiral pipe gives a very similar result to that observed in the straight pipe if the wall is an idealized rigid boundary. However, when coupling occurs [shown in Fig. 12(a) for steel and aluminum pipes], the sound speed measured in the pipe on both Earth and Venus differs significantly from the value that would be observed in an infinite 3D volume of atmosphere, or which would be predicted for a pipe with rigid walls.

While such acoustical sensors were initially proposed for measuring sound speeds, their layout would at first sight appear to be amenable to take attenuation data, and indeed this has been proposed in order to obtain the density of gas and the acoustic impedance through insertion loss.[46,48] Certainly, the atmospheric composition and conditions could be inferred from data on the acoustic absorption that occurs in the bulk atmosphere[32,52,53] (i.e., outside of the tube). Given however that Figs. 10, 11, and 12(a) showed that the sound speed of the gas in the pipes (straight and spiral) will differ from that in the bulk atmosphere (and earlier papers showed that the transducer resonance in the pipe will differ from that in the bulk atmosphere[44]), the question must be asked as to whether measured attenuations in the pipe can really be taken as representative of those in the bulk atmosphere. Figure 12(b) plots the attenuation coefficient taken by averaging the data from 500 microphones that are equally spaced on axis along the length of the tube (it is assumed in the simulation that they do not themselves attenuate the propagation). This number is probably unaffordable, but such averaging is required to obtain good data in the simulations for Venus conducted here, and it is possible that unacceptable scatter might occur with the use of only two fixed microphones (as with the proposition by Hanel and Strange that "Sound absorption is derived from the amplitudes of both microphones," although it is noted that the data were acceptable for the laboratory tests they conducted on Earth). Figure 12(b) shows that the simulated attenuation coefficient measured along the axis of a straight pipe (open circles) matches that of the bulk atmosphere[53] (solid line). However, the attenuation measured in the spiral pipe (asterisk symbols) differs greatly from that in the bulk atmosphere, because the walls will couple together adjacent gas layers in the spiral: not only does the presence of modes cause the sound speed and attenuation to differ from that found in the bulk gas, but propagation through non-rigid walls provides the signal with a "short-cut" so that it can miss out lengths of the fluid column and so not incur the travel time delay and absorption which would occur had it propagated entirely through the gas column. [The choice of aluminum for the pipe walls is illustrative only and does not imply this would be suitable for Venus' acidic atmosphere; the attenuation coefficient in Al is 0.1% that of the gas, and so is neglected (Table II)].

Therefore, if propagation within a vessel or pipe is to be used to determine gas properties through inversion of acoustic sound speed and attenuation, then if that inversion assumes propagation conditions in the free field, such an inversion could generate misleading results if the gas in question couples to the walls. The effect is enhanced for certain geometries (here, it was greater in the spiral pipe than the straight one). The effect is also greater for those materials where coupling is great, and the drive to reduce weight and save space in probes favors use of those sorts of materials and geometries. Choice of the excitation frequency can enhance or reduce the effects, and such choice (and corrections for coupling) can be undertaken using the approach outlined in this paper.

V. CONCLUSION

In this paper, a finite element method numerical study of acoustic wave propagation in liquid-filled viscoelastic pipes is conducted. Compared to theoretical and experimental studies, the numerical method provides an easy and reliable way to predict both propagation modes and attenuation in a liquid-filled pipe. Two particular applications are investigated in this paper. First, the pipeline system of the Spallation Neutron Source is simulated as a liquid-filled solid pipe. The results show agreements with the model developed by Baik *et al.*[7] Second, an acoustic planetary exploration sensor is investigated. Results show that, if coupling between pipe walls and gas inside is considered, a sensor calibrated on the Earth may not work appropriately on another planet, and this is illustrated using the example of a long-standing instrument designed for Venus and currently under consideration for the Jovian planets. The sound speed and attenuation measured even for Earth's atmosphere may not match those for an infinite 3D volume of gas for certain sensor geometries (e.g., a spiral pipe). The imperative to use lightweight materials and compact geometries in planetary probes will tend to exacerbate this effect. This coupling issue adds a second complication (the first being fluid loading[44]) to the use of pipe geometries for acoustical systems in dense atmospheres.

[1]E. Tohijima and T. Sato, "Nonlinear acoustical sounding system for detection of defects in pipelike objects," J. Acoust. Soc. Am. **83**, 1661–1666 (1988).

[2]J. M. Muggleton, M. J. Brennan, and R. J. Pinnington, "Wavenumber prediction of waves in buried pipes for water leak detection," J. Sound Vib. **249**, 939–954 (2002).

[3]T. G. Leighton, "What is ultrasound?" Prog. Biophys. Molec. Biol. **93**, 3–83 (2007).

[4]T. G. Leighton, "From seas to surgeries, from babbling brooks to baby scans: The acoustics of gas bubbles in liquids," Int. J. Modern Phys. B **18**, 3267–3314 (2004).

[5]G. T. Yim and T. G. Leighton, "Real-time on-line ultrasonic monitoring for bubbles in ceramic 'slip' in pottery pipelines," Ultrasonics **50**, 60–67 (2010).

[6]M. A. Ainslie and T. G. Leighton, "Near resonant bubble acoustic cross-section corrections, including examples from oceanography, volcanology, and biomedical ultrasound," J. Acoust. Soc. Am. **126**, 2163–2175 (2009).

[7]K. Baik, J. Jiang, and T.G. Leighton, "Acoustic attenuation, phase and group velocities in liquid-filled pipes: theory, experiment, and examples of water and mercury," J. Acoust. Soc. Am. **128**, 2610–2624 (2010).

[8]K. Baik, J. Jiang, and T. G. Leighton, "Theoretical investigation of acoustic wave propagation in a liquid-filled cylinder," ISVR Technical Report No. TR329, Institute of Sound and Vibration Research, University of Southampton, Southampton, UK, 2009.

[9]V. A. Del Grosso, "Analysis of multimode acoustic propagation in liquid cylinders with realistic boundary conditions: Application to sound speed and absorption measurements," Acustica **24**, 299–311 (1971).

[10]L. D. Lafleur and F. D. Shields, "Low-frequency propagation modes in a liquid-filled elastic tube waveguide," J. Acoust. Soc. Am. **97**, 1435–1445 (1995).

[11]C. R. Fuller and F. J. Fahy, "Characteristics of wave propagation and energy distributions in cylindrical elastic shells filled with fluid," J. Sound Vib. **81**, 501–518 (1982).

[12]A. R. Briscoe and R. J. Pinnington, "Axisymmetric vibrational power measurement in empty and fluid filled pipes," J. Sound Vib. **192**, 771–791 (1996).

[13]B. K. Sinha, T. J. Plona, S. Kostek, and S. Chang, "Axisymmetric wave propagation in fluid-loaded cylindrical shells," J. Acoust. Soc. Am. **92**, 1132–1155 (1992).

[14]V. N. R. Rao and J. K. Vandiver, "Acoustics of fluid-filled boreholes with pipe: Guided propagation and radiation," J. Acoust. Soc. Am. **105**, 3057–3066 (1999).

[15]R. Long, M. Lowe, and P. Cawley, "Attenuation characteristics of the fundamental modes that propagate in buried iron water pipes," Ultrasonics **41**, 509–519 (2003).

[16]J. E. Greenspon and E. G. Singer, "Propagation in fluids inside thick viscoelastic cylinders," J. Acoust. Soc. Am. **97**, 3502–3509 (1995).

[17]P. B. Nagy and A. H. Nayfeh, "Viscosity-induced attenuation of longitudinal guided waves in fluid-loaded rods," J. Acoust. Soc. Am. **100**, 1501–1508 (1996).

[18]L. Elvira-Segura, "Acoustic wave dispersion in a cylindrical elastic tube filled with a viscous liquid," Ultrasonics **37**, 537–547 (2000).

[19]T. G. Leighton, D.G. Ramble, A. D. Phelps, C. L. Morfey, and P. P. Harris, "Acoustic detection of gas bubbles in a pipe," Acust. Acta Acust. **84**, 801–814 (1998).

[20]T. G. Leighton, P. R. White and M. A. Marsden, "Applications of one-dimensional bubbles to lithotripsy, and to diver response to low frequency sound," Acta Acoust. **3**, 517–529 (1995).

[21]P. R. Birkin, T. G. Leighton, J. F. Power, M. D. Simpson, A. M. L. Vincotte, and P. Joseph, "Experimental and theoretical characterisation of sonochemical cells. Part 1. Cylindrical reactors and their use to calculate the speed of sound in aqueous solutions," J. Phys. Chem. A **107**, 306–320 (2003).

[22]P. R. Birkin, J. F. Power, A. M. L. Vincotte, and T. G. Leighton, "A 1kHz resolution frequency study of a variety of sonochemical processes," Phys. Chem. Chem. Phys. **5**, 4170–4174 (2003).

[23]B. Riemer, J. Haines, M. Wendel, G. Bauer, M. Futakawa, S. Hasegawa, and H. Kogawa, "Cavitation damage experiments for mercury spallation targets at the LANSCE-WNR in 2005," J. Nucl. Mater. **377**, 162–173 (2008).

[24]T. G. Leighton, J. Jiang, and K. Baik, "A TV demonstration of sound absorption connecting the space shuttle to submarines," Acoust. Bull. **36**(4), 35–40 (2011).

[25]B. R. Mace, D. Duhamel, M. J. Brennan, and L. Hinke, "Finite element prediction of wave motion in structural waveguides," J. Acoust. Soc. Am. **117**, 2835–2843 (2005).

[26]P. Stucky and W. Lord, "Finite element modeling of transient ultrasonic waves in linear viscoelastic media IEEE Transactions on Ultrasonics," Ferroelectric. Frequency Control **48**, 6–16 (2001).

[27]Z. You, M. Lusk, R. Ludwig, and W. Lord, "Numerical simulation of ultrasonic wave propagation in anisotropic and attenuative solid materials," IEEE Trans. Ultrasonics, Ferroelectron. Frequency Control **38**, 436–445 (1991).

[28]B. Hosten and C. Biateau, "Finite element simulation of the generation and detection by air-coupled transducers of guided waves in viscoelastic and anisotropic materials," J. Acoust. Soc. Am. **123**, 1963–1971 (2008).

[29]B. Hosten and M. Castaings, "FE modeling of Lamb mode diffraction by defects in anisotropic viscoelastic plates," NDT&E Int. **39**, 195–204 (2006).

[30]M. Castaings, C. Bacon, and B. Hosten, "Finite element predictions for the dynamic response of thermo-viscoelastic material structures," J. Acoust. Soc. Am. **115**, 1125–1133 (2004).

[31]"COMSOL Multiphysics User's Guide," Version 3.4, by COMSOL AB at http://www.comsol.com/ (last viewed 1 March 2011).

[32]H. E. Bass and J. P. Chambers, "Absorption of sound in the Martian atmosphere," J. Acoust. Soc. Am. **109**, 3069–3071 (2001).

[33]J. P. Williams, "Acoustic environment of the Martian surface," J. Geophys. Res. **106**, 5033–5041 (2001).

[34]T. G. Leighton, P. R. White and D. C. Finfer, "The sounds of seas in space (Invited Paper)," Proceedings of the International Conference on Underwater Acoustic Measurements, Technologies and Results, Heraklion, Crete, Greece, 833–840 (2005).

[35]T. G. Leighton and P. R. White, "The sound of Titan: A role for acoustics in space exploration," Acoust. Bull. **29**, 16–23 (2004).

[36]H. U. Eichelberger, K. Schwingenschuh, G. Prattes, B. Besser, Ö. Aydogar, I. Jernej, H. I. M. Lichtenegger, R. Hofe, P. Falkner, and T. Tokano, "Acoustics of planetary atmospheres with active multi-microphone techniques, probing Titan," Geophys. Res. Abstr. **10**, EGU2008-A-09049 (2008).

[37]M. C. Towner, J. R. C. Garry, R. D. Lorenz, A. Hagermann, B. Hathi, H. Svedhem, B. C. Clark, M. R. Leese, and J. C. Zarnecki, "Physical properties of the Huygens landing site from the surface science package acoustic properties sensor (API S)," Icarus **185**, 457–465 (2006).

[38]T. G. Leighton, D. C. Finfer, and P. R. White, "The problems with acoustics on a small planet," Icarus **193**, 649–652 (2008).

[39]S. Lee, M. Zanolin, A. M. Thode, R. T. Pappalardo, and N. C. Makris, "Probing Europa's interior with natural sound sources," Icarus **165**, 144–167 (2003).

[40]T. G. Leighton and A. Petculescu, "The sound of music and voices in space. Part 1: Theory," Acoust. Today **5**(3), 15–24 (2009).

[41]T. G. Leighton and A. Petculescu, "The sound of music and voices in space. Part 2: Modeling and simulation," Acoust. Today **5**(3), 25–27 (2009).

[42]T. G. Leighton and A. Petculescu, "Sounds in space: The potential uses for acoustics in the exploration of other worlds," Hydroacoustics **11**, 225–238 (2008).

[43]A. Hagermann, P. D. Rosenberg, M. C. Towner, J. R. C. Garry, H. Svedhem, M. R. Leese, B. Hathi, R. D. Lorenz, and J. C. Zarnecki, "Speed of sound measurements and the methane abundance in Titan's atmosphere," Icarus **189**, 538–543 (2007).

[44]T. G. Leighton, "Fluid loading effects for acoustical sensors in the atmospheres of Mars, Venus, Titan, and Jupiter," J. Acoust. Soc. Am. **125**, EL214–EL219 (2009).

[45]A. P. Zent, R. C. Quinn, and M. Madou, "A thermo-acoustic gas sensor array for photochemically critical species in the Martian atmosphere," Planet. Space Sci. **46**, 795–803 (1998).

[46]R. A. Hanel and M. G. Strange, "Acoustic experiment to determine the composition of an unknown planetary atmosphere," J. Acoust. Soc. Am.**40**, 896–905 (1966).

[47]R. A. Hanel, "Exploration of the atmosphere of Venus by a simple capsule," NASA Technical Note TN D-1909 (1964).

[48]D. Banfield, P. Gierasch, and R. Dissly, "Planetary descent probes: Polarization nephelometer and hydrogen ortho/para instruments," Proc. IEEE Aerosp. Conf. **2005**, 691–697 (2005).

[49]K. F. Herzfeld and T. H. Litovitz, *Absorption and Dispersion of Ultrasonic Waves* (Academic Press, New York, 1959).

[50]G. F. Lindal, G. E. Wood, H. B. Hotz, D. N. Sweetnam, V. R. Eshleman and G. L. Tyler, "The atmosphere of Titan: An analysis of the Voyager 1 radio occultation measurements," Icarus **53**, 348 (1983).

[51]A. D. Handford and L. N. Long, "The direct simulation of acoustics on Earth, Mars, and Titan," J. Acoust. Soc. Am. **125**, 640–650 (2009).

[52]A. Petculescu and R. M. Lueptow, "Fine-tuning molecular acoustic models: sensitivity of the predicted attenuation to the Lennard-Jones parameters," J. Acoust. Soc. Am. **117**, 175–184 (2005).

[53]A. Petculescu and R. M. Lueptow, "Atmospheric acoustics of Titan, Mars, Venus, and Earth," Icarus **186**, 413–419 (2007).

[54]M. Castaings, M. V. Predoi, and B. Hosten, "Ultrasound propagation in viscoelastic material guides," Proceedings of the Comsol Multiphysics user's conference, Paris, (2005), http://www.comsol.com/academic/papers/1003/ (Last viewed 23 March 2011).

[55]See supplemental material at http://dx.doi.org/10.1121/1.3598463 for two movie files. The first (Movie_Straight pipe.wmv) shows an axisymmetric simulation of propagation up a straight pipe with the dimensions and material properties shown in Fig. 1 of this paper. The axis of rotational symmetric is at the extreme left of the color plot, corresponding to the center-line of the pipe. The source generates an impulse signal at the bottom at $t = 0$s. This acoustic signal then propagates to the top of the pipe via the pipe walls and the liquid inside. Although only one main mode showed in the movie, the signal tends to be dispersive, because the speed of sound is frequency dependent (caused by coupling). The associated still figure (Still_straight pipe.jpg) shows a time history map of the signal along the center of the pipe. From the figure, only one main mode can be recognized. The fastest

wave front reaches the top of pipe (1.8 m) at about 1.3 s, while energy at frequencies with lower speed keeps catching up thereafter. The second movie file (Movie_Straight pipe with air annuli.wmv) repeats the conditions of (Movie_Straight pipe.wmv) but with the addition of 8 circles (0.1 mm in diameter) of gas halfway up the tube (which represent the cross sections of annular rings of gas because of the rotational symmetry). The annular rings introduced serious reflection inside the pipe. The associated still figure (Still_straight_pipe_with_air_annuli.jpg) shows a time history map of the signal along the center of the pipe. From the figure, part of the energy was reflected by the annular ring at about 0.07 s and re-reflected at the bottom at about 0.15 s. The reflection is serious, though only 8 very small size annular rings were introduced. In practice, millions of bubbles in the liquid will definitely make the situation (not only reflection, but also attenuation, etc.) more complicated. The movie file (Movie_ORNL_SNS_ pipes.wmv) shows a 3-D simulation of an acoustic pulse (pulse duration = 0.6 ms) propagating along a pipe system with same dimensions of the real Spallation Neutron Source TTF test loop used in ORNL. The pipe wall is steel, and the inside liquid is mercury. The associated still figure, a snapshot when $t = 2.5$ ms has been added to this paper as Fig. 8. The movie file (Movie_Spiral_Venus_aluminum_gas.avi) is an illustration of the simulation used to form Fig. 9 of this paper (the still of Fig. 9 shows more clearly, by marking the solid walls with additional hatching that cannot be put in the movie, that adjacent layers of the spiral alternate gas-solid-gas-solid, etc.). Transmission between gas layers, through the wall, allows pressure signals to propagate between the source (at the center of the spiral) and the furthest sensor (at the far end of the spiral) far more quickly than the actual propagation time for the signal which travels through the gas alone.